Arch. Metall. Mater. **63** (2018), 4, 1673-1682

DOI: 10.24425/amm.2018.125092

H. MOSTAAN*#, M. RAFIEI**

PREDICTION AND OPTIMIZATION OF MAGNETIC PROPERTIES OF LASER WELDED AISI 430 STAINLESS STEELS

The AISI 430 stainless steel with ferritic structure is a low cost material for replacing austenitic stainless steel because of its higher yield strength, higher ductility and also better polarisation resistance in harsh environments. The applications of AISI 430 stainless steel are limited due to insignificant ductility and some undesirable changes of magnetic properties of its weld area with different microstructures. In this research, a study has been done to explore the effects of parameters of laser welding process, namely, welding speed, laser lamping current, and pulse duration, on the coercivity of laser welded AISI 430 stainless steel. Vibrating sample magnetometery has been used used to measure the values of magnetic properties. Observation of microstructural changes and also texture analysis were implemented in order to elucidate the change mechanism of magnetic properties in the welded sections. The results indicated that the laser welded samples undergo a considerable change in magnetic properties. These changes were attributed to the significant grain growth which these grains are ideally oriented in the easiest direction of magnetization and also formation of some non-magnetic phases. The main effects of the above-mentioned factors and the interaction effects with other factors were evaluated quantitatively. The analysis considered the effect of lamping current (175-200 A), pulse duration (10-20 ms) and travel speed (2-10 mm/min) on the coercivity of laser welded samples.

Keywords: AISI 430, Response surface methodology, Laser welding, Magnetic properties

1. Introduction

Stainless steels with ferritic microstructure of ferritic stainless steels (FSS) which don't contain any nickel as an alloying element have moderate corrosion resistance with lower cost [1]. In the last decades, the diversity of FSS is becoming momentous in the market of stainless steel with an average share of 30% up from the less than 20% in the last century [2]. The microstructure of ferritic stainless steels can be fully ferritic or a mixture of ferrite and martensite structures where martensite lies in the grain boundaries [3]. The single phase stainless steel with fully ferritic microstructure can be provided by suppressing the formation of austenite phase at high temperatures. Grain boundary martensite can be formed either by austenite solid state transformation or during the last stage of solidification [3].

Ferritic stainless steels have excellent soft magnetic properties with high permeability, minimum residual magnetic flux density (M_r), low coercive force (H_c), and also great magnetic saturation flux density (M_s). Another essential factor to minimize the eddy current losses in AC magnet applications is electrical resistivity and fortunately ferritic stainless steels have very low electrical resistivity. These steels can be produced to very large dimensions in particular applications. The machinability of these steels is very good and are relatively inexpensive. They also exhibit lower expansion coefficient compared to austenitic stainless steels, which is a great advantage when temperature cycling resistance is needed [4]. Taking into account all of these features mean that stainless steels with ferritic or martensitic structures have been used in a wide range of magnetic applications [5].

Another exclusive application of these steels is making vessels for chemical and food industries, heat exchangers components, automotive and architectural design, etc [6]. Moreover, they can be used in electrical motors, in relays, and also generators [7].

For many of these applications, welding is a major procedure adopted for manufacturing of components. Though, ferritic stainless steel finds application in a very vast area yet it is restricted as a structural material because the fusion welding of the grade is associated with several challenges which are impact toughness and also the loss of ductility. These drawbacks can be attributed to the effect of the intense heat input associated with fusion welding processes which leads to grain growth in the heated section [2,8]. Also, fusion welding of this kind of stainless steels is accompanied precipitation of derogatory secondary phases particularly sigma phase in the heat affected zone and in the weld metal, which results in low toughness and ductility [9]. The σ-phase is the most serious of these secondary phases due to its effect on the corrosion resistance, mechanical properties or weldability of ferritic stainless steels among other properties.

* DEPARTMENT OF MATERIALS ENGINEERING AND METALLURGY, FACULTY OF ENGINEERING, ARAK UNIVERSITY, ARAK 38156-8-8349, IRAN
** ADVANCED MATERIALS RESEARCH CENTER, DEPARTMENT OF MATERIALS ENGINEERING, NAJAFABAD BRANCH, ISLAMIC AZAD UNIVERSITY, NAJAFABAD, IRAN
# Corresponding author: H-mostaan@araku.ac.ir

In order to prevent the formation of σ-phase, ferritic stainless steels must not be preheated over 400°C. Rapid cooling after welding of ferritic stainless steels is another solution [10]. The above-mentioned effects during fusion welding can be severely altered magnetic properties of material which in some cases the changes are unfavorable.

So, it is very important to choose a proper welding process and to control welding process parameters in order to minimize harmful effects of welding process on the magnetic properties of welded sections. Usual resistance welding processes and also gas tungsten arc welding methods are no longer proper for joining thin metallic sheets of stainless steel with ferritic structure. Since, these processes lead to excessive melting and undesirable heat affected zones. Grain coarsening and formation of the σ-phase can be controlled by applying processes which involve low heat input including laser beam welding, electron beam welding and solid state welding processes [11].

Welding by a laser beam is the ideal joining route for stainless steels because this process has a high power density and creates very narrow heat affected zone (HAZ).

Significant efforts have been done by various researchers in applying the laser welding methode to the welding of very thin sheets of stainless steel. For example, Ventrella and Berretta [12] studied the pulsed Nd: YAG laser welding of AISI 316L foils and the showed that the control of pulse energy is substantial in obtaining good quality welds and the process is very sensitive to the gap between to overlaid foils. In another work, they also used the same pulsed laser welding technique for the welding of Monel 400 foils with thickness of 100 μm [13]. In laser welding process, the quality of weld sections are the result of a combination of some parameters, such as travel speed, laser power, defocusing distance, shape of the pulse, pulse duration or pulse width, shielding gas and so on. Hence, the remarkable potential of the pulsed laser cannot be utilized without proper choosing of these parameters which mainly specify the temperature distribution of the laser-welded sections [14]. So, it is very critical to select laser welding parameters systematically for enhancing the weld bead properties.

To diminution labor endeavors, saving of time and cost, it is appropriate to predict and optimize laser welding parameters based on mathematical modeling. There are several methods for obtaining the favorable output variables by development of mathematical models. Responses surface method (RSM) is the best well-known type of design among experiment procedures.

This paper will investigate the main effects of laser welding on weldability, microstructure and magnetic properties of AISI 430 thin stainless steel.

Hence, 3 factors-5 levels experiments have been designed using response surface methodology design matrix and analyzing the responses of interest by a developed mathematical models based on experimental results. Finally, this paper aimed to optimize the parameters of laser welding process using response surface methodology to obtain the better magnetic properties in the welded zones.

2. Materials and experimental procedures

The experimental campaign was carried out by means of a IQI 400 Nd:YAG laser welding machine (with maximum output power of 400 W), whose main characteristics are mentioned in Table 1.

TABLE 1

Welding parameters used in this study

Pulse shape	Rectangular
Focal length (mm)	100
Beam spot size (mm)	0.18
Pulse repetition rate (Hz)	20
Laser light wavelength (nm)	1064

The weldments were prepared in dimensions of 100×50 ×0.4 mm^3 AISI 430 thin sheets in a lap joint configuration. The chemical composition of as-received material is given in Table 2.

TABLE 2

Chemical composition of the AISI 430 ferritic stainless steel (in wt%)

Elements	Fe	C	Cr	Mn	Mo	Si	S
wt%	81	0.11	16	1.25	0.58	1	0.06

The direction of welding was kept normal to the direction of rolling. A custom fixture was designed to guarantee the correct alignment and clamping of the specimens during the process. As mentioned, samples were lap jointed and during welding technically zero gaps between two sheets is maintained (See Fig. 1).

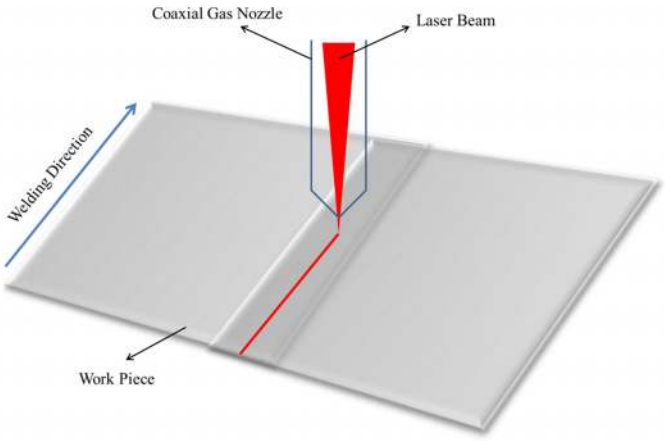

Fig. 1. Schematic illustration of laser welding set-up

Argon with 99.99999% purity was used for laser welding of AISI 430 ferritic stainless steel. The shielding gas was supplied to protect the top side of the weld form any possible contaminations. The coaxial argon shielding gas was applied by weld nozzle to protect weld pool. In order to prepare of the welded samples for microstructural evaluations by the mentioned methods in the standards, ASTME3, two transverse cross-sections

were separated from the weld zones by electrical discharge machining for all experiments. Samples for the metallographic observations have been prepared by polishing successively in, 180, 320, 400, 600, 800, 1200, 1600, 2000 grade emery papers to remove the scratches. After that, each sample was polished by 1 μm diamond paste. After performing the polishing with diamond paste, each of the samples is ready for etching. The composition of the etchant was dilute aqua regia (15 ml HCl, 5 ml HNO_3, and 100 ml H_2O at room temperature). Microstructure of the welded sections was examined using optical microscope (OM; Olympus BX50). X-ray diffraction (XRD) measurements were carried out using a Bruker 2D system, with Cr k_α radiation to determine the texture of the welded samples. The incomplete experimental pole figure data (pole figure of (110) and (200) planes) were used to calculate orientation distribution function (ODF) plots and inverse pole figures (IPFs) by TexTools software (RestMatCo.). The room temperature magnetic hysteresis (B-H) loops of the welded samples were measured by vibrating sample magnetometer (VSM, Meghnatis Kavir Kashan Co), vibration frequency: 82.5 Hz; Max. Field: 20KGauss; Moment range: 0.0001 emu to 50 emu. A 5×5 mm^2 specimen was cut from the welded samples in order to measure the magnetic properties.

The experimental campaign carried out in this work was based on the response surface method (RSM), according to which the three axes represent the parameters (lamping current, pulse duration and travel speed) involved in the experiments and any of them is delimited by two levels (maximum and minimum, as shown in Table 3). This approach, in particular, is called central composite design (CCD) and is based on a mathematical algorithm that calculates the eight intermediate cube points. In this way, the designed experiment presents the best characteristics in order to predict the effect of the varied parameters on the results achieved, to assess the variability of the process, to minimize the number of trials and to calculate mathematical formulas for the correlations of the process parameters with the results.

Statistical software MINITAB 16 was applied to establish the design matrix.

TABLE 3

Working range of laser welding parameters

Parameter	Pulse Duration (ms)	Lamping Current (A)	Travel Speed (mm/s)
Lower Limit	10	175	2
Upper Limit	20	200	10

3. Results and discussion

3.1. Microstructural and phase evolutions

The microstructural examination of pulsed Nd:YAG laser welded sections have been carried out using optical microscope. Figure 2a,b shows the typical microstructure of AISI 430 SS base metal and center of the weld metal, respectively.

As can be seen, the base metal microstructure is fully ferritic along with some carbide precipitates. The carbides are evenly distributed throughout the matrix. It is apparently observed that the average grain size of AISI 430 base metal is about 17±2 μm. Moreover, the grain size of weld metal is noticeably larger than that of base metal and has been reached up to 92±5 μm. The microstructure of the weld metal shows that melting started at the surface irradiates by the laser beam and the molten pool grows constantly to axial and radial direction. The welding conditions and microstructure of base metal (grain structure) have a great effect on fusion zone microstructure in epitaxial growth. Crystallographic characteristics will affect grain growth along especial directions, mainly the "easy growth" directions. For cubic materials the easy growth directions are <100>. In addition, no cellular or columnar grain growth can be seen even in the vacuity of fusion line. In other word, the variation of the G/R ratio (G is the temperature gradient and R is the growth rate) during solidification of the weld metal is negligible from fusion line to center line. Cellular or columnar growth structures form rather than equiaxed structure if the ratio between G and R is high.

The phase evaluations of laser welded AISI 430 SS were carried out by XRD analysis. The XRD patterns of the base metal

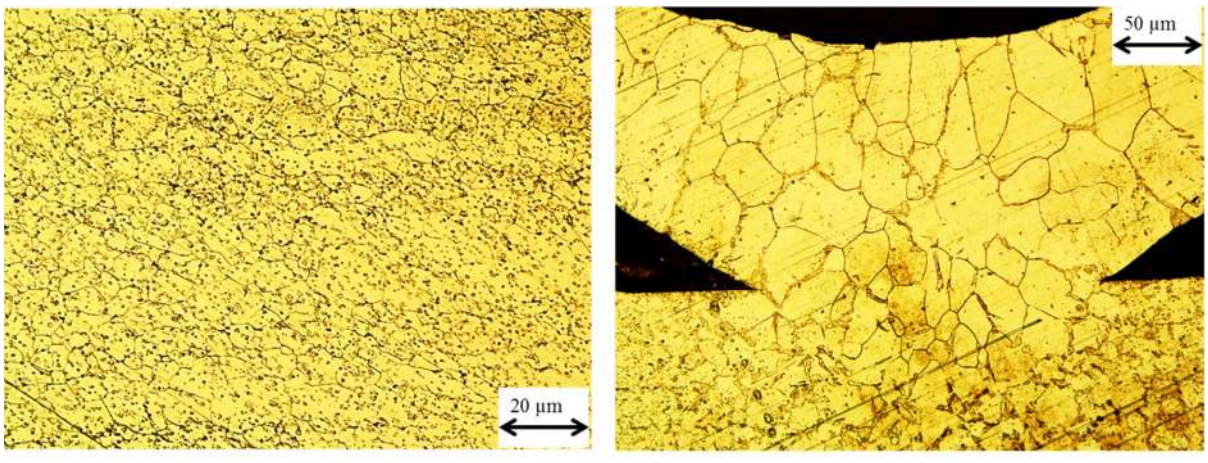

Fig. 2. Optical micrographs of (a) AISI 430 SS base metal; (b) center of the weld metal

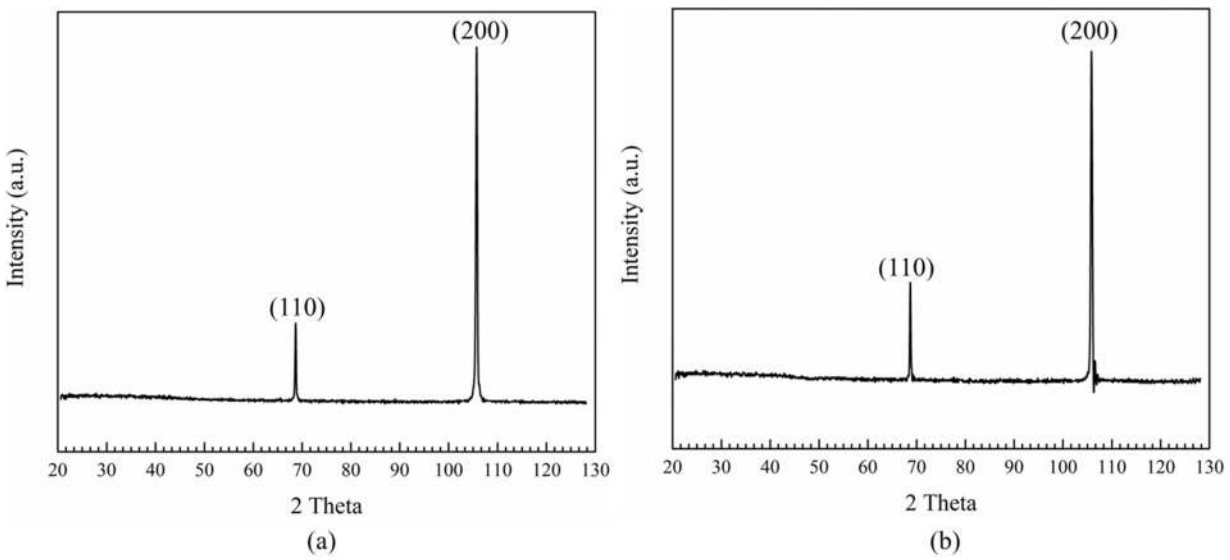

Fig. 3. XRD patterns of (a) base metal and (b) weld metal

and weld metal are shown in Fig. 3a,b. As can be seen, no new phase is formed during laser welding of AISI 430 SS and hence no phase evolution has been occurred during laser welding.

The weld appearances of two typical welded joints in AISI 430 SS produced by Nd:YAG laser are shown in Fig. 4. As can be seen, the macrostructure shows no solidification cracks or porosities. Thus, visible crack free lap joints with flawless weld bead geometry have been accomplished by autogenously laser welding of AISI 430 SS.

Fig. 4. Close view of two typical welded samples in lap joint configuration

3.2. Evolutions of magnetic properties

The changes of magnetic properties of laser welded samples were evaluated by means of VSM analysis. The magnetic hysteresis loops of the base metal and a typical welded sample are shown in Fig. 5.

Magnetic features such as remanence (B_r), coercive force (H_c) and saturation induction (B_s) are the main properties of soft magnetic materials. As shown in Fig. 5, hysteresis behavior may be explained by the motion of domain walls. Upon reversal of the field direction from saturation, the process by which the domain structure changes is reversed. There is a rotation of the single domain with the reversed field. After that, those domains that have magnetic moments aligned with the new field form and grow at the expense of the other domains. The resistance to movement of domain walls that occurs in response to the increase of the magnetic field in the opposite direction; this accounts for the lag of B with H, or the hysteresis. When the applied field reaches zero, there is still some net volume fraction of domains oriented in the former direction, which explains the existence of the remanence B_r. To reduce the B field within the specimen to zero, an H field of magnitude $-H_c$ must be applied in a direction opposite to that of the original field; H_c is called the coercivity, or sometimes the coercive force.

As shown in Fig. 5, the value of H_c for AISI 430 SS base metal is about 13.2 which has been decreased down to 5.8 after laser welding (for a typical welded sample). Coercivity (H_c), which also influences the shape of the hysteresis curve, is sensitive to structural variables rather than to chemical composition. For instance, a low value of coercivity corresponds to the easy movement of domain walls as the magnetic field changes magnitude and/or direction. Structural defects such as particles of a nonmagnetic phase or voids in the magnetic material, grain boundaries and degree of crystalline disordering tend to restrict the motion of domain walls and thus increase the coercivity. As mentioned previously, the grain size of the base metal has

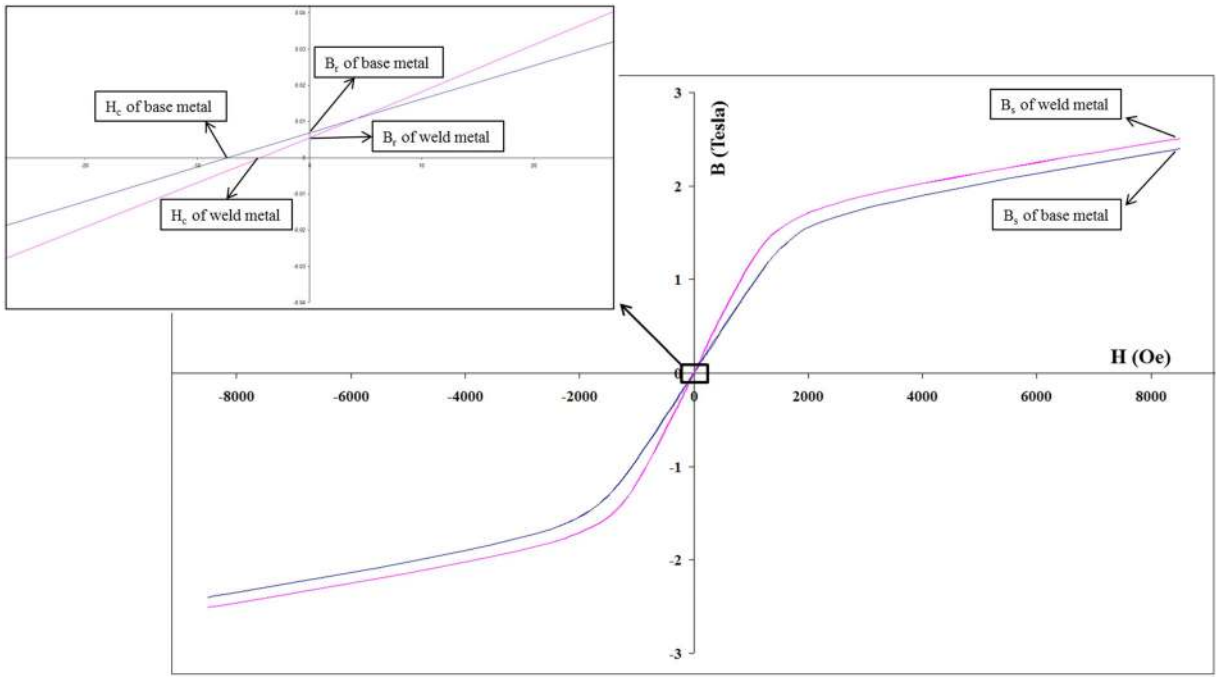

Fig. 5. VSM curves of base metal and weld metal showing the changes in B_s, B_r and H_c

been increased from ~17 μm up to ~93 μm after laser welding. It means that the density of grain boundaries is decreased by laser welding of AISI 430 base metal. So, we interpret this decrease in coercivity of AISI 430 base metal as due to larger grain size present in the weld metal. These large grains inhibit domain wall motion less effectively leading to softer magnetic properties. Another factor that can play a major role in affecting the coercivity value of AISI 430 base metal is formation of chromium carbide inclusions in the heat affected zone (due to the sensitization). These inclusions inhibit domain wall motion leading to harder magnetic properties. The influence of inclusions on the coercive force of ferromagnetic materials has been studied by many researchers [5]. But, as the results indicate, the impact factor of larger grain size is much higher than that of chromium carbide precipitation. Because the net effect of these two factors is decrease in coercivity value of welded samples. In addition, it can be concluded from Fig. 5 that the remanence value (value of the B field when $H = 0$) of AISI 430 base metal has been decreased from 1.5 down to 0.67. The value of Br is mainly governed by the orientation of grains. The magnetic properties of ferromagnetic materials, especially induction, are correlated with the easy and hard directions of magnetization in a particular crystal.

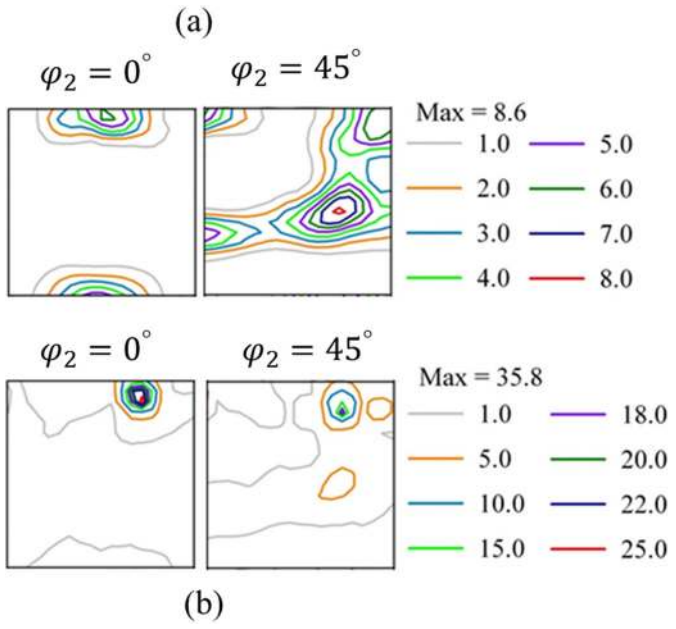

Fig. 6. Textures of the AISI 430 SS revealed by $\varphi_2 = 0°$ and 45° ODF sections, (a) in the as-received and (b) in the as-welded conditions

Fig. 6a,b shows the $\varphi_2 = 0°$ and 45° sections of orientation distribution functions (ODFs) for the AISI 430 SS in the as-received condition (base metal) and weld metal of a typical laser welded sample, respectively.

It is obvious that the texture of the base metal in Fig. 6a, has a dominant γ-fiber, some α-fiber components and also rotated cube texture component. γ-fiber represents components with crystallographic texture of <111>//ND. But after laser welding, the cube texture however has been diminished when α and γ-fibers completely disappear.

As shown above, the grain orientation of the base metal remarkably changes and a new texture is produced upon welding. This is important since residual flux density (B_r) can be severely affected by grains orientation.

The relevant texture components which evolve during thermomechanical processing of steels are aligned along the <110>//RD (α-fiber), $\{hhl\}\langle\frac{h}{l}+1\frac{h}{l}+2\frac{h}{2}\rangle$, ($\alpha$*-fiber), <100>//ND ($\theta$-fiber), <100>//RD ($\eta$-fiber) and <111>//ND ($\gamma$) fibers. However, the most frequently observed α, α* and γ-fibers texture

components, which evolve during both the hot and cold rolling operations, are unfavorable for magnetic properties since they have hard magnetization directions. In the case of materials which have a BCC crystal structure (such as AISI 430 SS), the <100> and <011> directions are the ones of easy magnetization while the <111> directions require more energy for saturation of the magnetic polarization [39]. For Instance, the γ and the <011>//ND fiber orientations have relatively high anisotropy energy and as such, the occurrence of these components in the soft magnetic material such as AISI 430 SS is undesirable. In the AISI 430 SS base metal which involve γ-fiber, some α-fiber components and also rotated cube texture component, magnetic moments can hardly rotate in the absence of magnetic field and consequently the Br value increases. This is due to this fact they have hard and medium magnetization directions. In contrast, as said before, after laser welding the cube texture however has been diminished when α and γ-fibers completely disappear. Formation of grains in the weld metal after laser welding with an enhanced orientation parallel to the easier magnetization direction results in lower resistance to changes of magnetization and therefore at $H = 0$ the value of B_r is low. So, decrease in B_r value in the AISI 430 base metal is a result of the disappearing texture components that have hard or medium magnetization direction. By analyzing the VSM data, it is revealed that the saturation induction (B_s) has been increased after laser welding of AISI 430 base metal. The maximum possible saturation induction B_s, of a ferromagnetic material represents the magnetization that results when all the magnetic dipoles in a solid piece are mutually aligned with the external field. The saturation induction or magnetization is determined only by the composition of the material. In the section of phase evolution it was discussed that there is some carbide precipitations which are evenly distributed in a ferritic matrix. These carbide precipitations are non-magnetic phases which decrease the saturation induction of AISI 430 base metal. But, after laser welding of AISI 430 base metal, probably these carbide precipitations cannot be formed in the weld metal because of rapid solidification of molten metal during laser welding. In this condition, carbide inclusions have not enough time to precipitate. So, decrease in volume fraction of carbide inclusions or absence of these inclusions during laser welding may be lead to increase in saturation induction.

3.3. Optimization of H_c values of the welded sheets

At the first step of optimization the important laser beam welding parameters that influence physical features (magnetic properties) of AISI 430 SS should be identified. From our laboratory experiments and based on studying the literature [26-28], the parameters which have a convincing influence on the physical properties of the welded sections were determined. These factors are lamping current, pulse duration and welding speed. Absolutely, the combinations of these factors will mainly specify the temperature distribution of the laser beam-welded samples.

- **Welding speed**

Welding speed is the predominant parameter in welding because which decides the productivity. It determines the type of welding mode (conduction or deep keyhole) and affects keyhole formation and stability. It influences the bead geometry particularly the depth of penetration.

- **Lamping current**

It is an important welding parameter to control the weld penetration depth. More the lamping current more will be the depth of penetration. If the lamping current is too high, spatter problem will arise and if it is too low, it will not fuse the metals resulting in a lack of fusion and lack of penetration defects. This parameter is varied and optimized to get the full penetration.

- **Pulse duration**

It is the pulsed laser beam exposure time over the metal surface. It is also called as the laser pulse width, measured in milliseconds (ms). It is the important parameter in pulsed welding which is used to fine-tune the weld bead geometry. Too low pulse width promotes spatter and too high pulse width causes overheating of the metal by conduction mode that is inefficient to fuse parts. So this parameter is optimized to produce tailored and stabilized defect free weld bead.

3.3.1. Determination the working limits of parameters

A large number of trial runs were carried out using 0.4 mm thick sheets of AISI 430 SS to find out practical working limits of laser beam welding parameters. Different combinations of welding parameters were used to carry out the trial runs. The nondestructive inspections were used to identify the working limits of the welding parameters. In all three standards, welds including cracks, incomplete penetration and incomplete fusion are not acceptable. The results obtained areas shown in Table 3.

TABLE 3

Coding and actual values of parameters

Parameters	Units	Symbols	Limits				
Lamping current	A	I	175	180.06	187.5	194.93	200
Welding speed	mm/s	S	2	3.62	6	8.37	10
Pulse duration	ms	T_p	10	12.02	15	17.97	20

3.3.2. Developing the design matrix and recording response

Twenty experiments for laser welding of AISI 430 SS have been conducted as per central composite rotatable design (CCD). Every experimental run was carried out respecting the order suggested by the RSM algorithm, as shown in Table 4.

TABLE 4

CCD design for actual factors and measured experimental results

Experimental details				Responses
Exp. No.	Factors			H_c (Oe)
	I	T_p	S	
1	180.06	12.02	3.62	7.3
2	180.06	17.97	3.62	7.1
3	194.93	12.02	3.62	6.8
4	194.93	17.97	3.62	5.1
5	180.06	12.92	8.37	6.1
6	180.06	17.97	8.37	7.3
7	194.93	12.92	8.37	7.25
8	194.93	17.97	8.37	7
9	187.5	10	6	7.6
10	187.5	20	6	6.7
11	175	15	6	7.1
12	200	15	6	5.9
13	187.5	15	2	6
14	187.5	15	10	7.15
15	187.5	15	6	7.1
16	187.5	15	6	7.09
17	187.5	15	6	7.1
18	187.5	15	6	7.08
19	187.5	15	6	7.08
20	187.5	15	6	7.012

3.3.3. Development of empirical relationship

RSM is accepted as a statistical route based on the multiple regressions. In the present investigation, the second-order RSM-based model was selected to estimate the responses as follow:

$$y = b_0 + \sum b_i x_i + \sum b_{ii} x_{ii}^2 + \sum b_{ij} x_i x_j + \varepsilon \qquad (1)$$

Where (b_0) is constant, (b_i), (b_{ii}) and (b_{ij}) represent the coefficients of linear, quadratic and interaction terms, respectively. (x_i) and (x_j) are the explicative variables and (ε) is a random experimental error. Thus, when the determined value of P corresponding to a coefficient exceeds the standard tabulated value for the desired level of confidence (~5%), the coefficient becomes infinitesimal. The results of analysis of variance (ANOVA) for the H_c are given in Table 5.

TABLE 5

ANOVA results for H_c value

Term	Coef	SE. Coef	T	P
Constant	7.076	0.065	108.61	0.000
T_p	–0.180	0.043	–4.173	0.002
I	–0.26	0.043	–6.214	0.000
S	0.24	0.043	5.56	0.000
$T_p \times T_p$	0.03	0.042	0.72	0.485
$I \times I$	–0.19	0.042	–4.735	0.001
$S \times S$	–0.17	0.042	–4.10	0.002
$T_p \times I$	–0.36	0.056	–6.52	0.000
$T_p \times S$	0.35	0.056	6.30	0.000
$I \times S$	0.41	0.6	7.414	0.000

Based on to the finding of ANOVA, the final mathematical model developed to predict the H_c values of laser beam welded joints is disposed below:

$$H_c = 7.076 - 0.18T_p - 0.26I + 0.24S - 0.19I^2 - 0.17S^2 - 0.36T_p \times I + 0.35T_p \times S + 0.41I \times S \qquad (2)$$

3.3.4. Validation of the optimum solutions generated by the model

The ability of the developed model in predicting the output values was examined using the ANOVA. ANOVA examination results for the developed model are reported in Table 6. The results of the ANOVA test showed that the regression is significant with linear, quadratic and interaction terms for the derived model.

The reliability of the derived model was probed by residual plots for H_c as shown in Fig. 7.

The normal probability plot of the residuals for coercivity (H_c), as illustrated in this figure, made known that the residuals are falling on a straight line, denoting normally distribution of errors.

TABLE 6

ANOVA test results for checking adequacy of the proposed model

Source	DF	Seq SS	Adj SS	Adj MS	F	P	Significance
Regression	9	7.49	7.49	0.833	44.08	0.000	✓
Linear	3	2.50	2.50	0.834	44.15	0.000	✓
Square	3	1.017	1.017	0.339	17.94	0.002	✓
Interaction	3	3.970	3.97	1.32	70.15	0.001	✓
Residual Error	10	0.189	0.189	0.189			
Lack-of-Fit	5	0.183	0.183	0.036	33.56	0.001	✓
Pure Error	5	0.005	0.005	0.001			
Total	19	7.68					
$R^2 = 96.33\%$							
SS: Sum of Square; MS: Mean Square; DF: Degree of Freedom.							

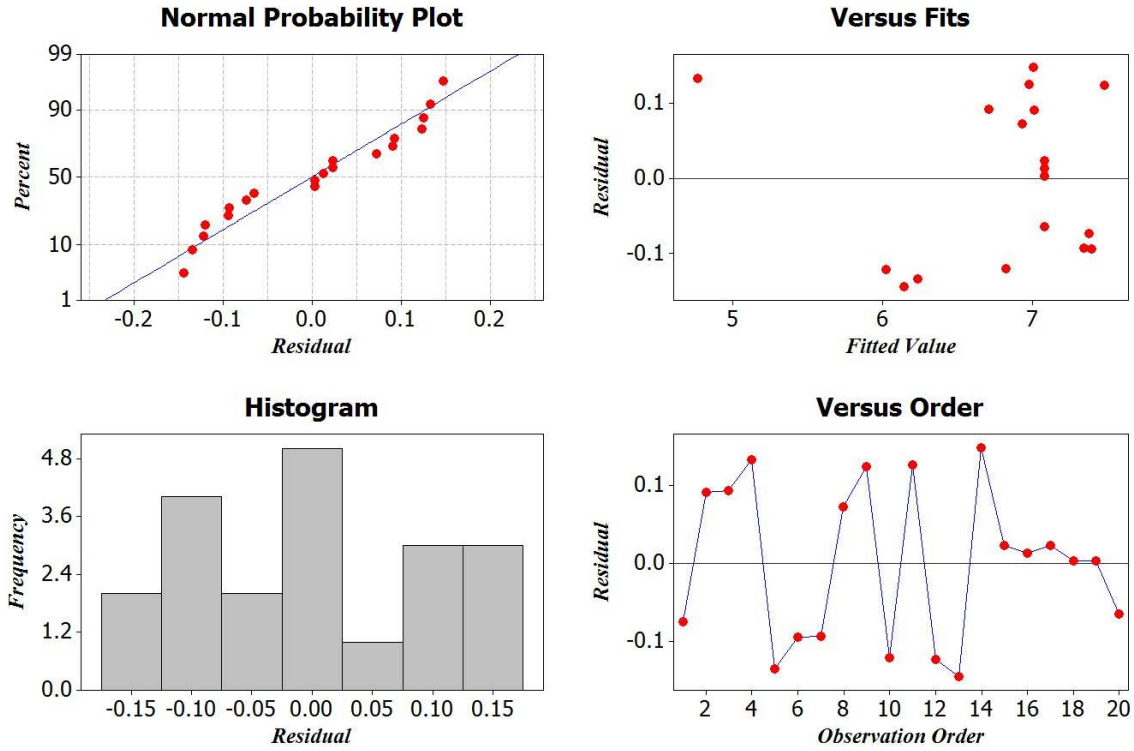

Fig. 7. Normal probability plots of H_c

The coefficient of determination 'R^2' is used to find how close the predicted and experimental values lie [15]. For a theoretically perfect statistical model, the value of R^2 is 1. This coefficient of determination (R^2) was calculated to be 0.9633 for the response of H_c which indicates that the model can predict 96.33% of the experimental data and leave only 3.67% of the total variations as unexplained. All above considerations confirm the competence of the developed model.

3.3.5. The effects of process parameters on the response

The main effects of different process variables on the H_c, as guessed from the mathematical relationship, are displayed in Fig. 8.

In general, the Fig. 8 shows almost persuasive trends between the cause and the result. Accordingly, based on the

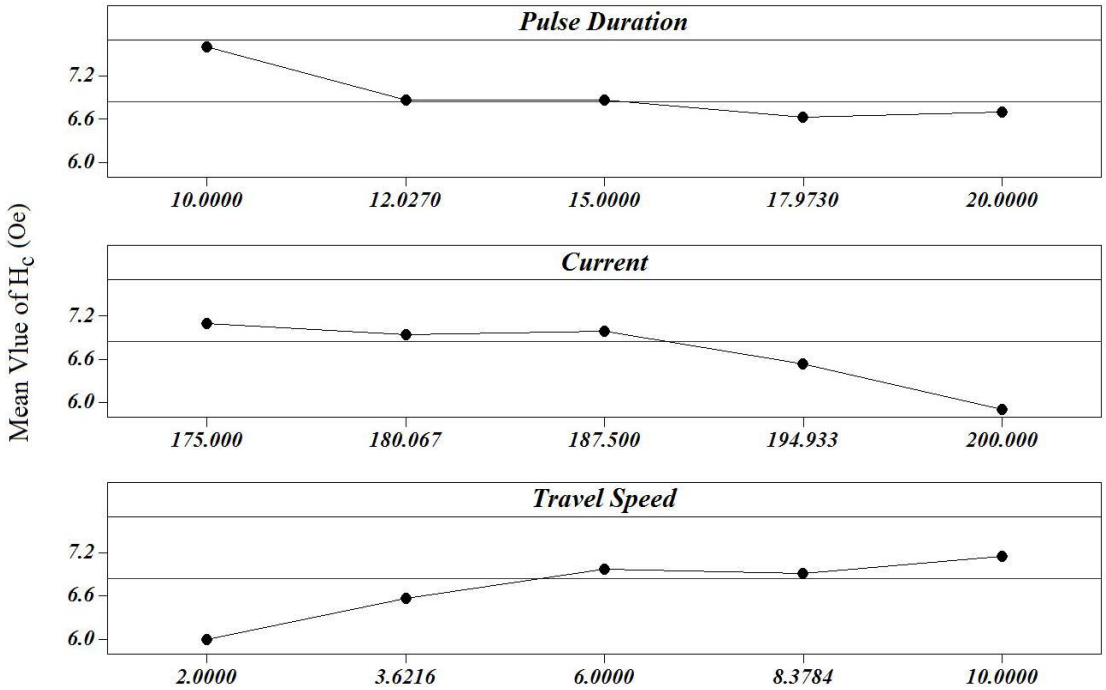

Fig. 8. Plots of the main effects of different variables on the H_c response

conducted tests, it can be concluded that the utmost significant laser processing parameters are travel speed (S) and lamping current (I), while the pulse duration is a less important process parameter. Also, it is obvious that by increasing the values of pulse duration and lamping current, the H_c values of laser weld joints have been decreased. In contrast, travel speed has a direct effect on the vales of H_c i. e. increase in travel speed gives rise to increase in H_c values of welded samples.

In the laser beam welding process, the pulse energy or the heat delivered to the specimen is shown by E_p and can be calculated through the following equation:

$$\text{Pulse energy (J)} = \text{Pulse duration (ms)} \times \times \text{Average peak power (kw)} \quad (3)$$

From the above equation, it can be said that by increase in pulse duration, the energy transferred to the sample is increased and hence a larger area is affected by the laser beam leading to formation a larger weld area. As discussed above, decrease in the H_c and B_r value during laser beam welding is a result of grains growth in the weld metal which these grains are ideally oriented parallel to the easier direction of magnetization. As a result, one can assume that increase in welded section area is associated with extension of an area with the large grain size. Thus, it is anticipated that increase in the welded zone area leads to decrease of H_c value. Increase in lamping current leads to increase in average peak power which has an effect similar to pulse duration on the heat input and hence H_c values of the welded samples. Increase in travel speed (S) leads to decrement in weld bead size. This is because of laser beam traveling at high speed over the welding seam when travel speed is increased. So, the value of heat input decreases, causing less volume of the parrent metal being melted. As a result, the size of the welded sections decreases. This implies that by the increase in travel speed value, the section with the diminished values of coercivity decreases.

- **Interaction effect of lamping current and pulse duration H_c**

Fig. 9 gives the contour plots of the interaction effects of pulse duration and lamping current. This figure shows that the H_c values for the laser welded samples are low at high pulse duration and lamping current. The increase in the magnitude of pulse duration (T_p) increases the heat input per unit length of the joint, causing more weld area. On the other hand, the increase in lamping current (from 175 to 200 A) lead to decrease in H_c value. Also, the decreasing trend of H_c with increase in pulse duration increases with increase in lamping current.

- **Interaction effect of pulse duration (T_p) and travel speed (S) H_c**

Counter plot which shows the interaction effects of pulse duration and travel speed is demonstrated in Fig. 10. From this figure, it is evident that H_c increases with increase in travel speed, whereas it decreases with increase in pulse duration. These effects are because of this fact that travel speed has a positive effect but pulse duration has a negative effect on H_c. By decrease in pulse duration and increase in the value of travel speed, the delivered heat input to the AISI 430 base metal decreases. Therefore, a smaller weld metal will be establish in this condition.

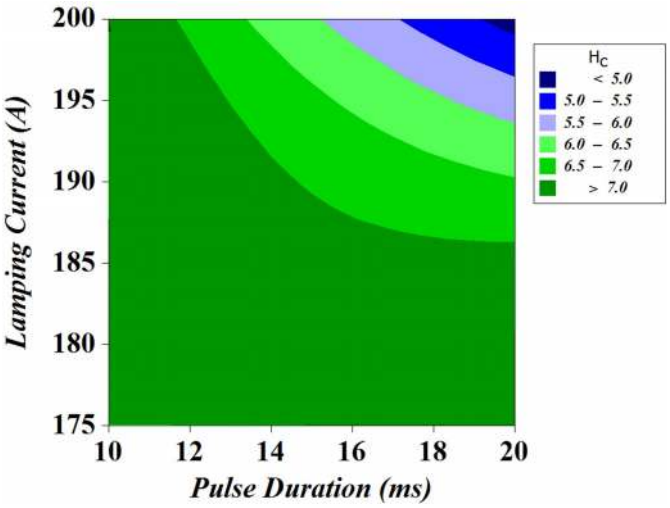

Fig. 9. Interaction effect of lamping current (I) and pulse duration (T_p) on H_c value of the welded samples

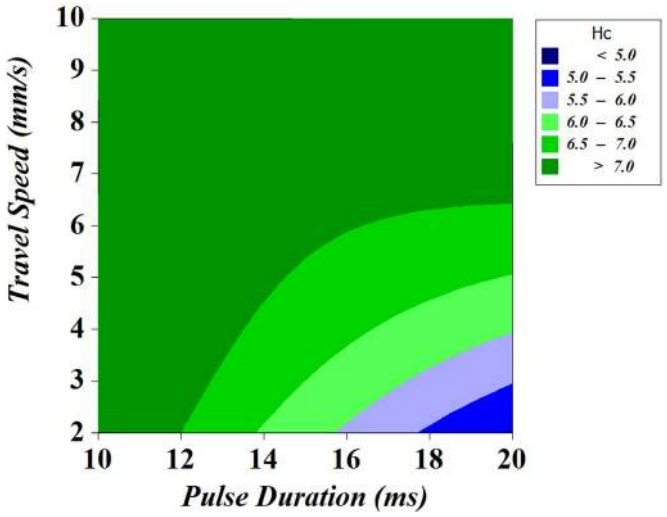

Fig. 10. Interaction effect of pulse duration (T_p) and travel speed (S) on H_c value of the laser welded samples

- **Interaction effect of lamping current and travel speed H_c**

Figure 11 shows the contour plots of the interaction effects of travel speed and lamping current on H_c. It is explicit that the value of H_c increases with increase the value of travel speed, but it decreases with increase in lamping current.

Hence the increasing trend of H_c with increasing of travel speed increases with increase in lamping current.

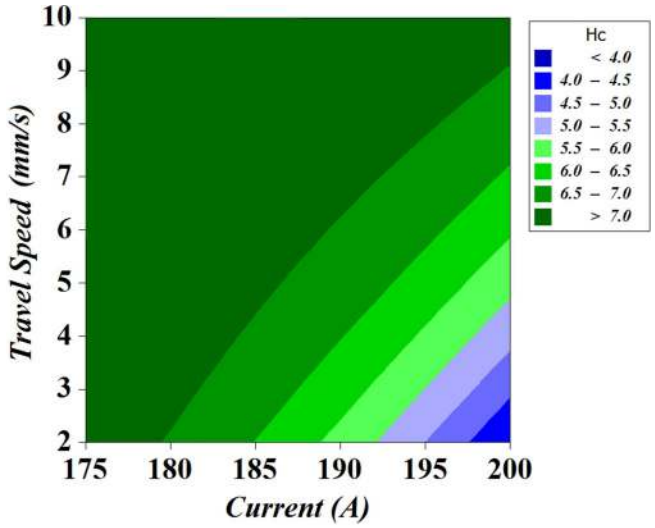

Fig. 11. Interaction effects of lamping current and travel speed on H_c value of the laser welded samples

4. Conclusions

Some conclusions can be drawn from this investigation:

1 – Laser welding of AISI 430 stainless steel (which is ferritic) leads to formation of large exuiaxed grains in weld area which their size is about 93 μm which larger than that of base metal (17 μm).

2 – Laser welding of AISI 430 stainless steel leads to decrease in the values of coercivity (H_c) and remanence (B_r) and increase in saturation induction.

3 – Decrease in coercivity was attributed to the formation of large grains in the weld area, while formation of grains in the weld metal which are preferably oriented in the easiest direction of magnetization was the main reason which is responsible for decrease in remnence value.

4 – Formation of some non-magnetic phase such carbide inclusions was assumed the most probable reason for increase in the value of saturation induction.

5 – The utmost significant laser welding parameters are travel speed and the magnitude of lamping current, while the pulse duration is a less important process parameter.

6 – By increasing the values of pulse duration and lamping current, the coercivity values of laser welded joints have been decreased. In contrast, travel speed has a direct effect on the vales of coercivity.

REFERENCES

[1] G. Mallaiah, P.R. Reddy, A. Kumar, Procedia Mater. Sci. **6**, 1740-1751 (2014).

[2] M.O.H. Amuda, S. Mridha, Mater. Des. **47**, 365-371 (2013), doi:10.1016/j.matdes.2012.12.008.

[3] K.D. Lippold JC, Welding metallurgy and weldability of stainless steels, John Wiley & Sons, New Jersey, 2005.

[4] K.D. Ramkumar, A. Chandrasekhar, A.K. Singh, S. Ahuja, A. Agarwal, N. Arivazhagan, A.M. Rabel, J. Manuf. Process. **20**, 54-69 (2015).

[5] P. Oxley, J. Goodell, R. Molt, J. Magn. Magn. Mater. **321**, 2107-2114 (2009).

[6] G. Mallaiah, A. Kumar, P. Ravinder Reddy, G. Madhusudhan Reddy, Mater. Des. **36**, 443-450 (2012).

[7] L. Battistini, R. Benasciutti, A. Tassi, J. Magn. Magn. Mater. **133**, 603-606 (1994).

[8] M.O.H. Amuda, S. Mridha, Adv. Mater. Res. **86**, 1165-1172 (2010).

[9] M.B. Bilgin, C. Meran, O.E. Canyurt, Int. J. Adv. Manuf. Technol. **77**, 2221-2233 (2014).

[10] S. Kou, Welding Metallurgy, 2003. doi:10.1016/0022-4596 (88)90042-4.

[11] M. Alizadeh-Sh, S.P.H. Marashi, M. Pouranvari, Mater. Des. **56**, 258-263 (2014).

[12] V.A. Ventrella, J.R. Berretta, W. de Rossi, J. Mater. Process. Technol. **210**, 1838-1843 (2010).

[13] V.A. Ventrella, J.R. Berretta, W. de Rossi, Phys. Procedia. **12**, 347-354 (2011).

[14] Q. Han, D. Kim, D. Kim, H. Lee, N. Kim, J. Mater. Process. Technol. **212**, 1116-1122 (2012).

[15] R. Myers, D. Montgomery, C. Anderson-Cook, Response surface methodology: process and product optimization using designed experiments, John Wiley & Sons, New Jersey, 2009.